

Effect of Temperature on Li-rich Layered Cathode Material $0.5\text{Li}_2\text{MnO}_3 \cdot 0.5\text{LiNi}_{0.5}\text{Mn}_{0.5}\text{O}_2$ Prepared by a Low Temperature Solution Combustion Synthesis

Shaoping Feng^{1,2}, Xin Kong^{1,2}, Hongyan Sun^{1,2}, Baosen Wang^{1,2}, Yin He^{1,2}, Guiyang Liu^{1,2,*}

¹ Department of Chemistry, College of Science, Honghe University, Mengzi, 661199, Yunnan, China

² Local Characteristic Resource Utilization and New Materials Key Laboratory of Universities in Yunnan, Honghe University, Mengzi 661199, Yunnan, China.

*E-mail: liuguiyang@tsinghua.org.cn

Received: 4 June 2018/ Accepted: 23 July 2018 / Published: 1 September 2018

Li-rich layered cathode materials of $0.5\text{Li}_2\text{MnO}_3 \cdot 0.5\text{LiNi}_{0.5}\text{Mn}_{0.5}\text{O}_2$ were synthesized by a low temperature solution combustion synthesis method. The effects of different ignition temperatures on the phase composition and electrochemical performances of the materials were studied. The results reveal that all the materials of $0.5\text{Li}_2\text{MnO}_3 \cdot 0.5\text{LiNi}_{0.5}\text{Mn}_{0.5}\text{O}_2$ are of ordered layered structure and maintain a similar morphology with homogeneous and polyhedral particles. Electrochemical experiments indicated that the $0.5\text{Li}_2\text{MnO}_3 \cdot 0.5\text{LiNi}_{0.5}\text{Mn}_{0.5}\text{O}_2$ obtained at a ignition temperature of 500 °C showed the higher discharge capacity of 220.2 mAh·g⁻¹ at 0.1 C and the capacity retention rates of 91.1 % after 50 cycles as well as excellent rate capability than that of other samples. The capacity retention rates of the samples ignited at 400 °C, 500 °C and 600 °C are more than 90%, and the sample ignited at 400 °C shows the best electrochemical cycling stability during cycling. It is concluded that ignition temperature has an important effect on the electrochemical performances of Li-rich layered cathode materials of $0.5\text{Li}_2\text{MnO}_3 \cdot 0.5\text{LiNi}_{0.5}\text{Mn}_{0.5}\text{O}_2$.

Keywords: Li-rich layered cathode material, Lithium ion batteries, $0.5\text{Li}_2\text{MnO}_3 \cdot 0.5\text{LiNi}_{0.5}\text{Mn}_{0.5}\text{O}_2$, Low temperature solution combustion synthesis

1. INTRODUCTION

Li-rich layered cathode materials of $x\text{Li}_2\text{MnO}_3 \cdot (1-x)\text{LiMO}_2$ materials have attracted great interests due to their high capacity (> 250 mAh·g⁻¹), good safety and low cost [1, 2]. However, they also have several drawbacks, including low coulombic efficiency, rapid capacity loss and poor cycling stability[3]. To improve the electrochemical performances of $x\text{Li}_2\text{MnO}_3 \cdot (1-x)\text{LiMO}_2$ materials, synthetic methods optimization(microwave synthesis[4], the polyvinyl alcohol assisted sol-gel

method[5], coprecipitation-hydrothermal-calcination method[6], the seed-mediated method[7], et al.[8]), structure design(3D hierarchical architectures[9], hierarchical micro/nanostructure[10], hierarchically-structured nanocrystalline[11], et al.[2]), surface modification(various coatings with MgO[12], Al₂O₃[13], Y₂O₃[14], Li₂ZrO₃[15], FeF₃[16], MoS₂[17], Li₃PO₄[18], et al.[19, 20]) and element doping (Fe[21], Mg[22], Ca[23], Ti[24], et al.[25]) have been explored.

In our previous work, We have reported LiNi_{0.5}Mn_{1.45}Zn_{0.05}O₄[26], 3D porous LiNi_{0.5}Mn_{1.5}O₄[27], LiNi_{0.5}Mn_{1.5-x}Cu_xO₄[28], LiNi_{0.5}Mn_{1.49}Zr_{0.01}O₄[29] and porous LiMn₂O₄[30] prepared by solution combustion synthesis method, which the materials with excellent electrochemical performances can be synthesized at lower temperature and in shorter time. In this paper, a series of 0.5Li₂MnO₃·0.5LiNi_{0.5}Mn_{0.5}O₂ materials have been synthesized by a low temperature solution combustion synthesis method, and the effects of different ignition temperatures on the phase composition and electrochemical performances of the material were studied.

2. EXPERIMENTAL

2.1 Preparation

About 12 g raw materials of CH₃COOLi, LiNO₃, (CH₃COO)₂Mn, Mn(NO₃)₂, (CH₃COO)₂Ni and Ni(NO₃)₂ with the stoichiometric ratios of 0.6:0.6:0.3:0.3:0.1:0.1 were dissolved in 7.5 mL distilled water to obtain uniform solution. The solution was ignited and combusted at different temperatures(400°C, 500°C, 600 °C and 700 °C) in the muffle furnace for 2h and then cooled in air, forming the brown-black powders. The 0.5Li₂MnO₃·0.5LiNi_{0.5}Mn_{0.5}O₂ materials were synthesized after calcinated at 800 °C for 12h and cooled naturally in the muffle furnace. For convenience, The samples were recorded as 400-800, 500-800, 600-800 and 700-800, respectively.

2.2 Characterization

The phase composition and morphologies of the samples were ascertained by power X-ray diffraction (XRD, PANalyticalX'pert pro, Cu-K α radiation) and scanning electron microscopy (SEM, FEI Quanta FEG 250).

2.3 Electrochemical performance test

The electrochemical performances of the 400-800, 500-800, 600-800 and 700-800 samples were tested in CR2025 coin cells with Li metal foil as negative electrode, which were assembled in a high purity Ar-filled glove-box. 1.0M LiPF₆ dissolved in ethylenecarbonate (EC)/ dimethylcarbon (DMC) (1:1 v/v), Celgard 2400 polyethylene membrane was used as electrolyte and separator, respectively. The cathode electrodes were fabricated by mixing 80 wt.% 0.5Li₂MnO₃·0.5LiNi_{0.5}Mn_{0.5}O₂ material, 10 wt.% carbon black and 10wt.% polyvinylidene difluoride

(PVDF) dissolved in N-methyl-2pyrrolidone (NMP). A battery test system (LAND CT2001A) was used to test the electrochemical performance of the CR2025 coin cells at different C rates ($1\text{ C}=150\text{ mA}\cdot\text{g}^{-1}$) within the range from 2.0 to 5.0 V. The electrochemical impedance spectroscopy (EIS) within the range from 100 kHz to 0.1 Hz was measured by the electrochemical workstation of CHI 660.

3. RESULTS AND DISCUSSION

3.1 Phase composition

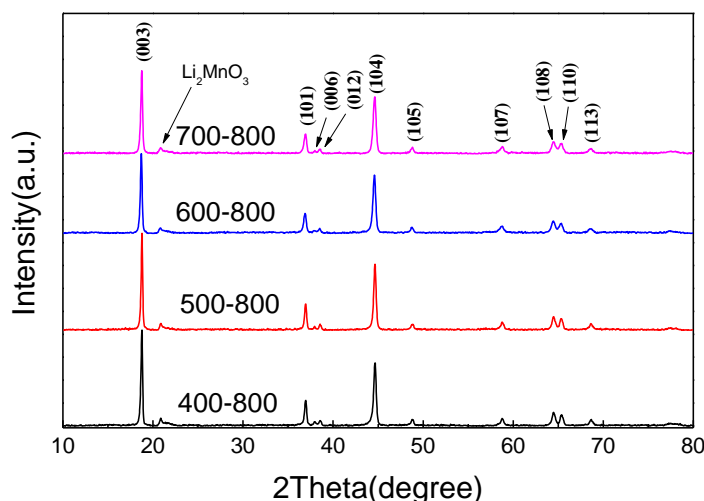


Figure 1. XRD patterns of the 400-800, 500-800, 600-800 and 700-800 samples

Fig. 1 shows the XRD patterns of $0.5\text{Li}_2\text{MnO}_3\cdot 0.5\text{LiNi}_{0.5}\text{Mn}_{0.5}\text{O}_2$ at different ignition temperatures. As shown in Fig.1, the peaks of (006)/(102) and (108)/(110) are clearly separated, indicating that all the samples are of ordered layered structure[31, 32]. Moreover, a few weak peaks at $20\text{-}22^\circ(2\theta)$ are ascribed to Li_2MnO_3 phase.

Table 1 Lattice parameters of the 400-800, 500-800, 600-800 and 700-800 samples

Samples	a (Å)	c(Å)	c/a	I(003)/I(104)
400-800	2.8539	14.2085	4.979	1.53
500-800	2.8532	14.2042	4.978	1.49
600-800	2.8534	14.2340	4.988	1.40
700-800	2.8535	14.2291	4.986	1.49

Table 1 lists the lattice parameters, c/a ratios and I(003)/I(104) ratios, which are similar to documents[33]. Obviously, the I(003)/I(104) ratios of 400-800, 500-800, 600-800 and 700-800 samples are more than 1.2, meaning that all the samples possess a low cation mixing[34].

3.2 Morphology

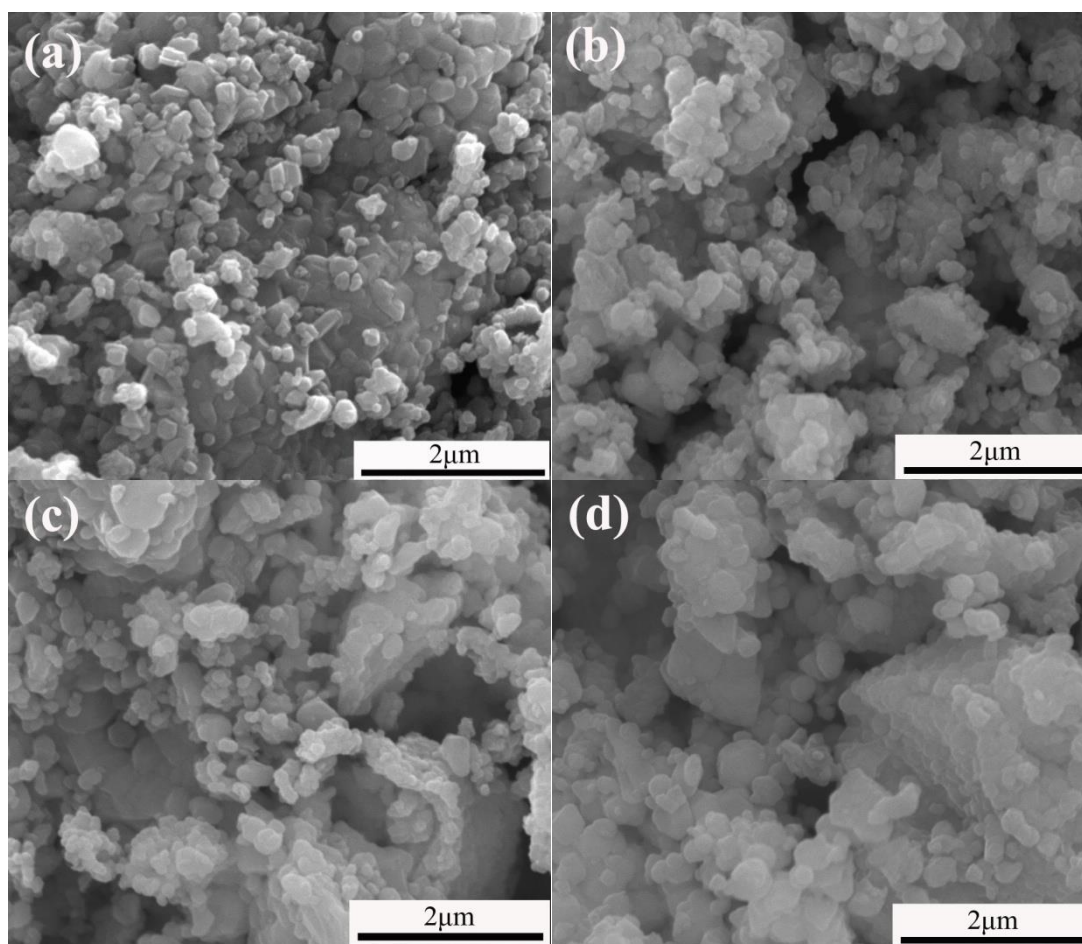


Figure 2. SEM images of the 400-800 (a), 500-800 (b), 600-800 (c) and 700-800 (d) samples at different magnifications

The SEM images of 400-800, 500-800, 600-800 and 700-800 samples at different magnifications are shown in Fig. 2. All the samples maintain a similar morphology with homogeneous and polyhedral particles, but the particle size is different. With the increasing of ignition temperature, the particle size increases.

3.3 Electrochemical performance

The initial charge-discharge curves of 400-800, 500-800, 600-800 and 700-800 samples are displayed in Fig. 3. There are two charge platforms at about 4.0 and 4.5 V during the initial charge process, which are correlated with the oxidation processes of Ni^{2+} to Ni^{4+} and the extraction from the phase of Li_2MnO_3 , respectively[35]. The initial discharge capacity of 400-800, 500-800, 600-800 and 700-800 samples is 188.7, 220.2, 202.7 and 181.2 $\text{mAh}\cdot\text{g}^{-1}$ with coulombic efficiency of 80.2, 80.1, 77.6 and 74.3 %, respectively. Compared with the first charge-discharge curves, 500-800 sample has higher discharge capacity and coulombic efficiency than that of other samples reported previously [13,

36-39].

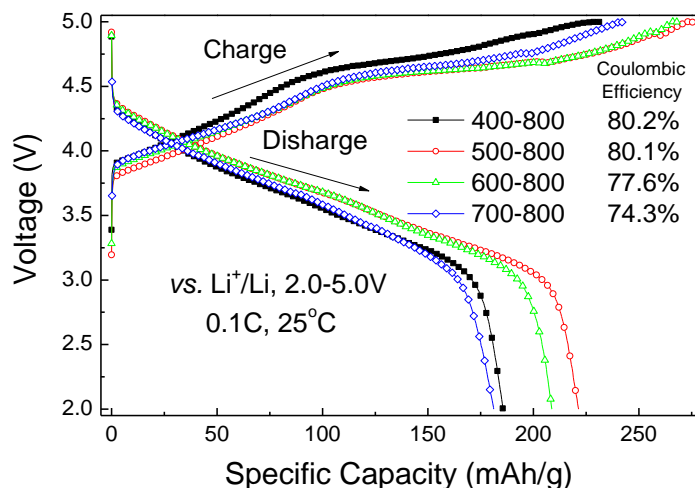


Figure 3.The initial charge-discharge curves of the 400-800, 500-800, 600-800 and 700-800 samples

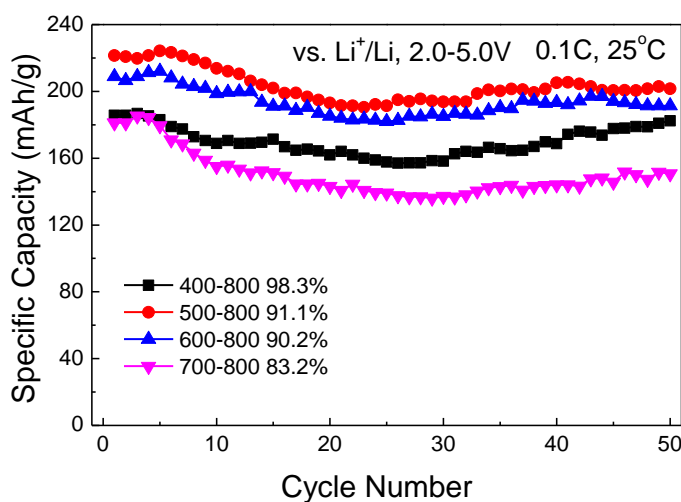


Figure 4.The cycling performances of the 400-800, 500-800, 600-800 and 700-800 samples

Fig. 4 compares the cycling performances of 400-800, 500-800, 600-800 and 700-800 samples at 0.1C in 2.0-5.0 V after 50 cycles. The capacity retention rates of 400-800, 500-800, 600-800 and 700-800 after 50 cycles are 98.3 %, 91.1 %, 90.2 % and 83.2 %, respectively. It can be seen that the capacity retention rates of the samples decrease apparently with the increase of ignition temperature. The capacity retention rates of 400-800, 500-800 and 600-800 are more than 90%, and 400-800 sample shows the best electrochemical cycling stability during cycling.

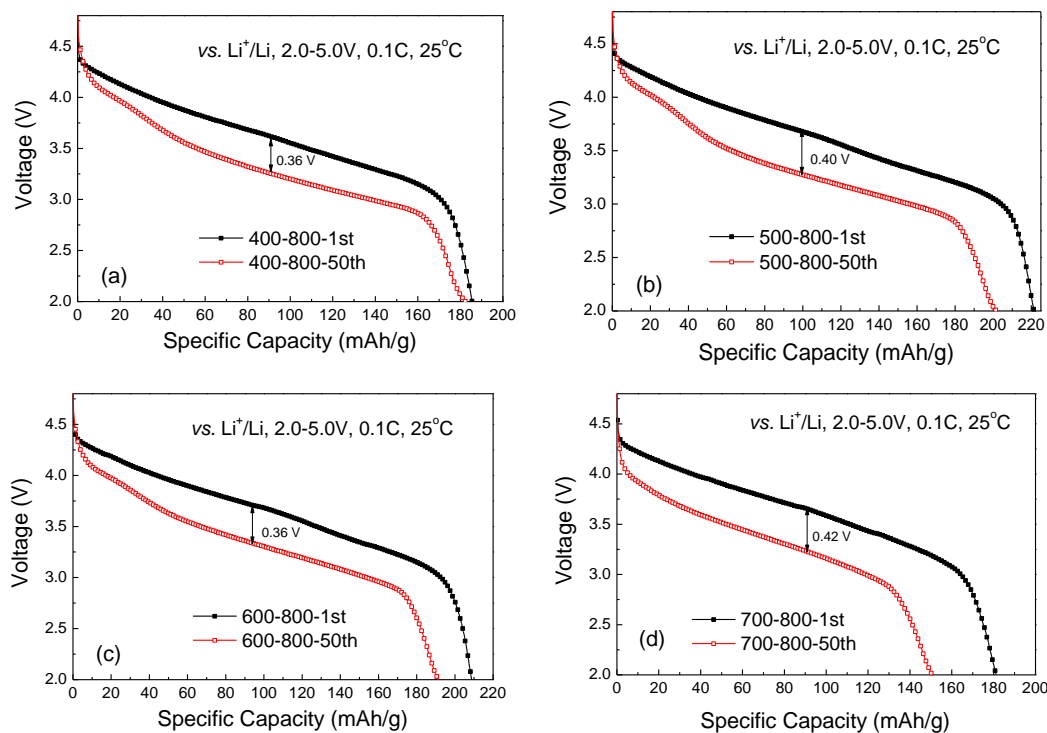


Figure 5. The discharge curves of the 1st cycle and the 50th cycle of the 400-800, 500-800, 600-800 and 700-800 samples.

Discharge curves of the 1st and 50th cycles for the samples 400-800, 500-800, 600-800 and 700-800 samples at 0.1C are exhibited in Fig. 5. Apparently, there was obvious voltage fade during cycling of all the samples, but 700-800 sample was much more severe than that of other samples.

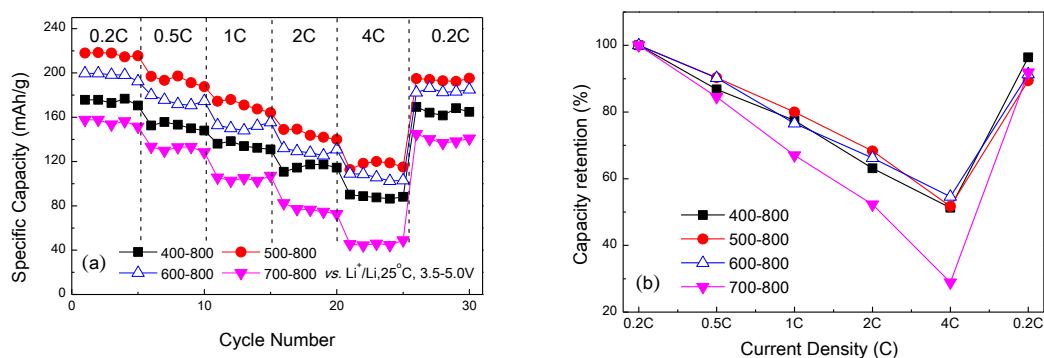


Figure 6. The rate capabilities (a) and the capacity retentions (b) of the 400-800, 500-800, 600-800 and 700-800 samples.

The rate capabilities of the 400-800, 500-800, 600-800 and 700-800 samples are presented in Fig. 6 (a) and Fig. 6 (b). It can be seen that the rate capability of 500-800 is the best among them, and then 600-800, followed by 400-800, and the worst is 700-800. With the increase of ignition temperature, the rate capabilities of 500-800, 600-800 and 700-800 decreased, which can be ascribed to the relatively larger particles at a higher ignition temperature. The larger particles of the materials,

the longer diffusion pathways of lithium ions during cycling under the same conditions, which can lead to poor rate capabilities[40, 41]. Moreover, the rate capability of 500-800 and 600-800 are close to or higher than those of other Li-rich layered cathode materials [42, 43].

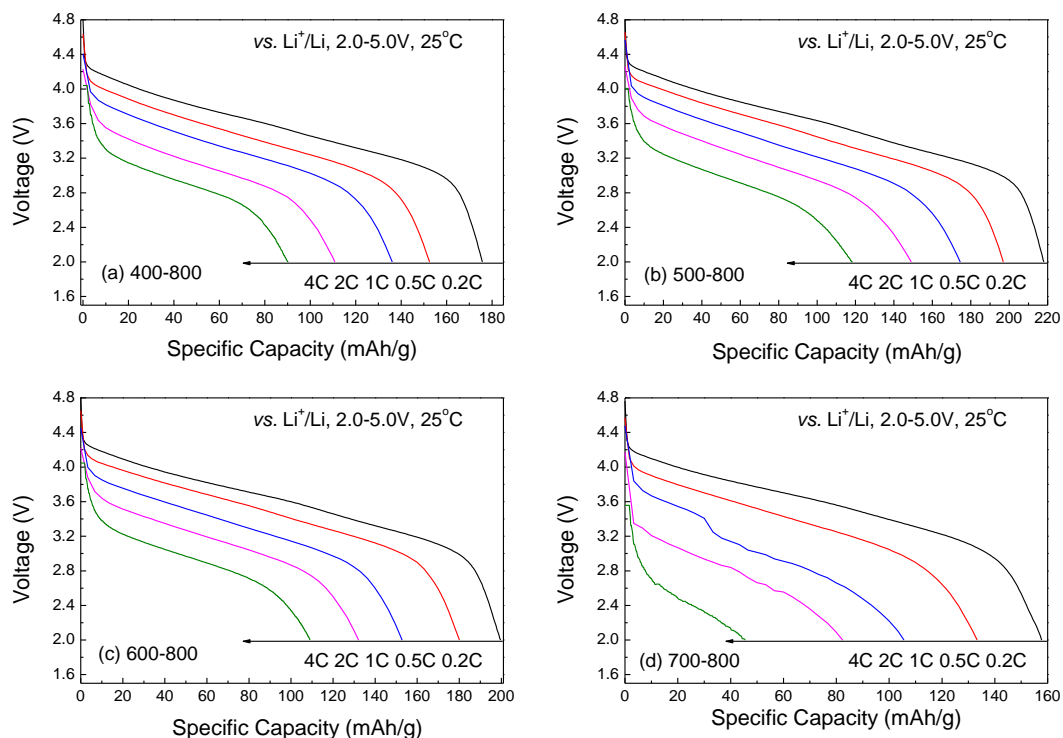


Figure 7. Discharge curves of (a) 400-800, (b) 500-800, (c) 600-800 and (d) 700-800 samples at various C rates between 2.0 and 5.0 V.

Fig. 7 show the discharge curves of the 400-800, 500-800, 600-800 and 700-800 samples at various C rates. It is clear that the discharge voltage of all the samples decreases with the increase of C rate, especially for the sample 700-800, which is deliver their capacity of 45.5 mAh·g⁻¹ at 4.0 C and remains 28.9 % capacity.

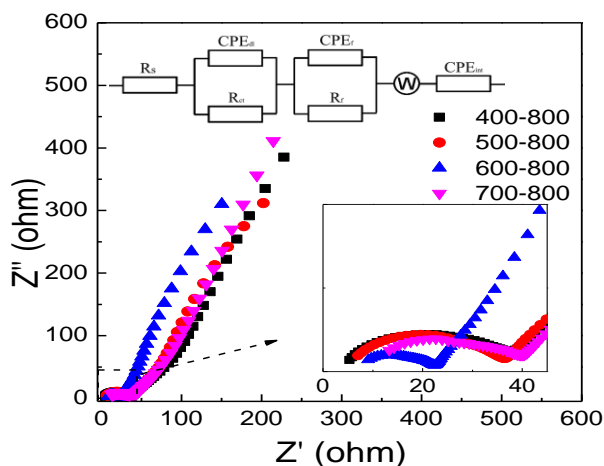


Figure 8.EIS spectra of the 400-800, 500-800, 600-800 and 700-800 samples in 0.1Hz-100kHz range after 3rd cycles.

To understand the variation of the electrochemical performance for the samples, the EIS spectra and the corresponding equivalent circuit are shown in Fig. 8. In this equivalent circuit, R_s , R_f and R_{ct} corresponds to the electrolyte resistance, the Li^+ migration resistance and the charge transfer resistance, respectively[44, 45]. It appears that the R_{ct} of 500-800 and 600-800 is smaller than that of 400-800 and 700-800, indicating that the former possesses lower electrochemical polarization[21]. It is a possible reason that the samples of 500-800 and 600-800 have superior rate capability than that of other samples, which are consistent with the rate capability analysis results above.

4. CONCLUSIONS

In the work, a series of Li-rich layered cathode materials of $0.5\text{Li}_2\text{MnO}_3 \cdot 0.5\text{LiNi}_{10.5}\text{Mn}_{0.5}\text{O}_2$ ignited at different temperatures of 400 °C, 500 °C, 600 °C and 700 °C were successfully prepared by a low temperature solution combustion synthesis method. All the as-synthesized samples with ordered layered structures had a similar morphology, but the particles size became larger with the increase of ignition temperature. Electrochemical experiments indicated that 500-800 sample delivered initial discharge capacity of $220.2 \text{ mAh} \cdot \text{g}^{-1}$ at 0.1 C and a capacity retention rate of 91.1 % after 50 cycles as well as excellent rate capability, which are superior than that of other samples. The 400-800 sample exhibited excellent electrochemical cycling stability and maintain 98.3% of capacity retention rates at 0.1 C after 50 cycles. The above-mentioned results concluded that the electrochemical performance of $0.5\text{Li}_2\text{MnO}_3 \cdot 0.5\text{LiNi}_{10.5}\text{Mn}_{0.5}\text{O}_2$ can be improved with proper ignition temperature, which can be attributed to particle size and structural stability of the materials.

ACKNOWLEDGEMENT

This work was supported by the National Natural Science Foundation of China (No. 51662007 and No. U1602273) and the Key Construction Disciplines of Chemistry for Master Degree Program in Yunnan.

References

1. S.M. Zhang, T. Tang, Z.H. Ma, H.T. Gu, W.B. Du, M.X. Gao, Y.F. Liu, D.C. Jian, H.G. Pan, *J. Power Sources*, 380 (2018) 1-11.
2. M. Xu, L.F. Fei, W. Lu, Z.Y. Chen, T. Li, Y. Liu, G.Y. Gao, Y.Q. Lai, Z.A. Zhang, P. Wang, H.T. Huang, *Nano Energy*, 35 (2017) 271-280.
3. C.H. Jiang, Z.M. Zou, *Electrochim. Acta*, 269 (2018) 196-203.
4. S.J. Shi, S.S. Zhang, Z.J. Wu, T. Wang, J.B. Zong, M.X. Zhao, G. Yang, *J. Power Sources*, 337 (2017) 82-91.
5. Y.H. Xiang, Z. Sun, J. Li, X.W. Wu, Z.X. Liu, L.Z. Xiong, Z.Q. He, B. Long, C. Yang, Z.L. Yin, *Ceram. Int.* 43 (2017) 2320-2324.
6. M.H. Tabuchi, H.Y. Kageyama, K.J. Takamori, Y.C. Imanari, K.J. Nakane, *Electrochim. Acta*, 210 (2016) 105-110.
7. H.Z. Zhang, Y.T. Zhang, D.W. Song, X.X. Shi, L.Q. Zhang, L.J. Bie, *J. Alloys Compd.*, 709 (2017) 692-699.
8. G.B. Liu, H. Liu, Y.F. Shi, *Electrochim. Acta*, 88 (2013) 112-116.

9. D.T. Ma, Y.L. Li, M.S. Wu, L.B. Deng, X.Z. Ren, P.X. Zhang, *Acta Materialia*, 112 (2016) 11-19.
10. F. Fu, Y.P. Deng, C.H. Shen, G.L. Xu, X.X. Peng, Q. Wang, Y.F. Xu, J.C. Fang, L. Huang, S.G. Sun, *Electrochem. Commun.*, 44 (2014) 54-58.
11. Y.C. Jin, J.G. Duh, *Energy Storage Mater.* 6 (2017) 157-163.
12. S.J. Shi, J.P. Tu, Y.Y. Tang, X.Y. Liu, Y.Q. Zhang, X.L. Wang, C.D. Gu, *Electrochim. Acta*, 88 (2013) 671-679.
13. S.Y. Liu, Z.L. Wang, Y.K. Huang, Z.J. Ni, J.R. Bai, S.F. Kang, Y.G. Wang, X. Li, *J. Alloys Compd.*, 731 (2018) 636-645.
14. Q.C. Chen, L.M. Luo, L. Wang, T.F. Xie, S.C. Dai, Y.T. Yang, Y.P. Li, M.L. Yuan, *J. Alloys Compd.*, 735 (2018) 1778-1786.
15. H.M. Liang, Z.X. Wang, H.J. Guo, J.X. Wang, J. Leng, *Appl. Surf. Sci.* 423 (2017) 1045-1053.
16. C.D. Li, J. Xu, J.S. Xia, W. Liu, X. Xiong, Z.A. Zheng, *Solid State Ionics*, 292 (2016) 75-82.
17. J.Z. Kong, C.L. Wang, X. Qian, G.A. Tai, A.D. Li, D. Wu, H. Li, F. Zhou, C. Yu, Y. Sun, D. Jia, W.P. Tang, *Electrochim. Acta*, 174 (2015) 542-550.
18. Z.Y. Wang, S.H. Luo, J. Ren, D. Wang, X.W. Qi, *Appl. Surf. Sci.* 370 (2016) 437-444.
19. H.Z. Zhang, T.H. Yang, Y. Han, D.W. Song, X. Shi, L.Q. Zhang, L.J. Bie, *J. Power Sources*, 364 (2017) 272-279.
20. L.N. Cong, X.G. Gao, S.C. Ma, X. Guo, Y.P. Zeng, L.H. Tai, R.S. Wang, H.M. Xie, L.Q. Sun, *Electrochim. Acta*, 115 (2014) 399-406.
21. T.F. Yi, Y.M. Li, X.D. Cai, S.Y. Yang, Y.R. Zhu, *Materials Today Energy*, 4 (2017) 25-33.
22. X. Jin, Q.J. Xu, H.M. Liu, X.L. Yuan, Y.Y. Xia, *Electrochim. Acta*, 136 (2014) 19-26.
23. C.P. Laisa, R.N. Ramesha, K. Ramesha, *Electrochim. Acta*, 256 (2017) 10-18.
24. X. Feng, Y.R. Gao, L.B. Ben, Z.Z. Yang, Z.X. Wang, L.Q. Chen, *J. Power Sources*, 317 (2016) 74-80.
25. C. Lu, S.Q. Yang, H. Wu, Y. Zhang, X.J. Yang, T.H. Liang, *Electrochim. Acta*, 209 (2016) 448-455.
26. H.Y. Sun, X. Kong, B.S. Wang, T.B. Luo, G.Y. Liu, *Int. J. Electrochem. Sci.*, 12 (2017) 8609-8621.
27. S.P. Feng, X. Kong, H.Y. Sun, B.S. Wang, T.B. Luo, G.Y. Liu, *Int. J. Electrochem. Sci.*, 13 (2018) 4276-4284.
28. H.Y. Sun, X. Kong, B.S. Wang, T.B. Luo, G.Y. Liu, *Ceram. Int.* 44 (2018) 4603-4610.
29. S.P. Feng, X. Kong, H.Y. Sun, B.S. Wang, T.B. Luo, G.Y. Liu, *J. Alloys Compd.*, 749 (2018) 1009-1018.
30. G.Y. Liu, X. Kong, Y.N. Li, B.S. Wang, *Materials Technology*, 31 (2016) 299-306.
31. H.X. Meng, L.Q. Li, J.Q. Liu, X.P. Han, W.G. Zhang, X.J. Liu, Q. Xu, *J. Alloys Compd.*, 690 (2017) 256-266.
32. K. Gao, S.X. Zhao, S.T. Guo, C.W. Nan, *Electrochim. Acta*, 206 (2016) 1-9.
33. S.K. Chong, Y.F. Wu, Y.Z. Chen, C.Y. Shu, Y.N. Liu, *J. Power Sources*, 356 (2017) 153-162.
34. Y.K. Zhou, P.F. Bai, H.Q. Tang, J.T. Zhu, Z.Y. Tang, *J. Electroanal. Chem.*, 782 (2016) 256-263.
35. G.F. Xu, Q.R. Xue, J.L. Li, Z.Y. Li, X.P. Li, T.H. Yu, J.G. Li, X.D. Wang, F.Y. Kang, *Solid State Ionics*, 293 (2016) 7-12.
36. Y.Q. Wu, J. Ming, L.H. Zhuo, Y.C. Yu, F.Y. Zhao, *Electrochim. Acta*, 113 (2013) 54-62.
37. D. Li, H.Z. Zhang, C.W. Wang, D. Song, X.X. Shi, L.Q. Zhang, *J. Alloys Compd.*, 696 (2017) 276-289.
38. R.N. Ramesha, C.P. Laisa, K. Ramesha, *Electrochim. Acta*, 249 (2017) 377-386.
39. X.P. Zhang, S.W. Sun, Q. Wu, N. Wan, D. Pan, Y. Bai, *J. Power Sources*, 282 (2015) 378-384.
40. G.F. Xu, J.L. Li, X.P. Li, H.W. Zhou, X.N. Ding, X.D. Wang, F.Y. Kang, *Electrochim. Acta*, 173 (2015) 672-679.
41. F. Li, Y.Y. Sun, Z.H. Yao, J.S. Cao, Y.L. Wang, S.H. Ye, *Electrochim. Acta*, 182 (2015) 723-732.
42. P.H. Yang, H.L. Li, X. Wei, S.C. Zhang, Y.L. Xing, *Electrochim. Acta*, 271 (2018) 276-283.
43. L. Li, Y.L. Chang, H. Xia, B.H. Song, J.R. Yang, K.S. Lee, L. Lu, *Solid State Ionics*, 264 (2014) 36-44.

44. C. Ghanty, R.N. Basu, S.B. Majumder, *Solid State Ionics*, 256 (2014) 19-28.
45. C.C. Wang, Y.C. Lin, K.F. Chiu, *J. Alloys Compd.*, 721 (2017) 600-608.

© 2018 The Authors. Published by ESG (www.electrochemsci.org). This article is an open access article distributed under the terms and conditions of the Creative Commons Attribution license (<http://creativecommons.org/licenses/by/4.0/>).